

Article

Design and Experiment of a Plateau Data-Gathering AUV

Hao Xu , Guo-Cheng Zhang *, Yu-Shan Sun *, Shuo Pang, Xiang-Rui Ran and Xiang-Bin Wang

Science and Technology on Underwater Vehicle Laboratory, Harbin Engineering University, Harbin 150001, China; xuhao0619@hrbeu.edu.cn (H.X.); sspp27@hotmail.com (S.P.); ranxiangrui@hrbeu.edu.cn (X.-R.R.); 2010011501@hrbeu.edu.cn (X.-B.W.)

* Correspondence: zhangguocheng@hrbeu.edu.cn (G.-C.Z.); sunyushan@hrbeu.edu.cn (Y.-S.S.)

Received: 11 September 2019; Accepted: 17 October 2019; Published: 21 October 2019



Abstract: The design, control, and implementation of an autonomous underwater vehicle (AUV) for collecting hydrological information from plateau rivers and lakes are presented in this paper. The hardware and software structures of the control system were previously described. A novel sliding mode controller (SMC) with combinational reaching law of vertical hovering motion is proposed to improve the robustness and stability. The S-plane control, a nonlinear controller with little parameters, is used in the horizontal motion. Besides, the navigation strategy based on the dead-reckoning algorithm, a path tracking based on the light-of-sight (LOS) algorithm, and a control allocation strategy considering saturation are present. Finally, experiments were performed in a tank and in a river in the Qinghai–Tibet Plateau to prove the feasibility and reliability of the AUV system.

Keywords: AUV; control system; sliding-mode controller; hovering

1. Introduction

The Qinghai–Tibet Plateau, as the source of numerous rivers in East Asia, Southeast Asia, and South Asia, plays an important role in the Asian region. In recent years, the Qinghai–Tibet Plateau has experienced some ecological problems, such as glacial retreat, rising snow lines, and shrinking lakes [1] due to global warming and insufficient environmental protection. Regular inspections and observations of the waters are important for protecting the ecology and studying global climate change. Traditionally, manual monitoring is usually the main method for inspection and observation. However, it is an extremely dangerous, laborious, and time-consuming task due to high altitude, extreme cold, and low oxygen [2]. Hence, efficiency and quality are usually limited.

With the development of marine vehicles and sensors technology, unmanned underwater vehicles are more and more widely used in scientific, commercial military, and other fields due to its ability to carry different sensors [3], such as submarine pipeline monitoring [4–6], submarine resources detection [7,8], marine environment monitoring [9,10], seafloor mapping [11,12], etc. Various tasks that are difficult for humans to approach can be performed by unmanned underwater vehicles (UUVs) in waters. Usually, UUVs can be divided into ROVs (remotely operated vehicles) and AUVs (autonomous underwater vehicles). An ROV is controlled by the operator to perform underwater tasks via a cable. However, manual operations are highly dependent on the skill and experience of the operator. More importantly, the operation range and the task efficiency of ROV are limited due to the configuration of signal cables. Traditional torpedo-shaped AUVs are more flexible than ROVs because they are cable-free. This allows them to perform wide range and long-term ocean surveys. Since conventional torpedo-shaped AUVs are driven by a combination of thrusters and rudders, they cannot be hovered to keep the AUV at the same depth. In recent years, many research teams have developed H-AUVs with

hovering capability to meet diverse underwater mission requirements, such as submarine hydrothermal observation [13], underwater image mosaicking [14], and seafloor observation [15].

Hovering observation is an important part of hydrological monitoring. Inspired by the above research, an AUV is developed for plateau hydrological data collection. The AUV is small and lightweight so that it is easy to deploy and operate. It has the performance of a torpedo-shaped AUV and the capability of hovering for long autonomy in shallow water (100 m). The following are the key features of the AUV:

- 1) Efficient hydrodynamics and long endurance;
- 2) A hovering capability which is suitable for most tasks;
- 3) Lightweight and easy operation, which can be operated by two persons;
- 4) Well extendibility, which can be equipped with various sensors.

Underwater vehicle motion is highly nonlinear and strongly coupled, and thus, its hydrodynamic parameters are difficult to obtain accurately. Moreover, the AUV has a slender body, therefore controlling its pitch angle and depth is a challenging task compared to ROVs. The AUV's antenna is exposed to the water surface to ensure normal communication in the state of floating on the water surface. When the AUV dives, extra buoyancy is completely generated by the antenna, and the vertical force and pitch angle moments are simultaneously generated. The difficulty of vertical motion control will be further increased. This is a challenge for controller design.

In recent decades, several control techniques have been proposed, such as linear controllers [16,17], fuzzy logic control [18,19], predictive control [20,21], SMC controllers [22], and neural network-based control [23]. These have performed satisfactorily. In terms of robustness, SMC is superior to other control techniques [24]. The SMC can ensure perfect control performance in the presence of uncertain parameters or models. It has the advantages of having a simple control algorithm and excellent dynamic performance, which is suitable for engineering practice. However, there are also deficiencies in conventional SMC. Firstly, the conventional SMC ensures the system converges to the equilibrium points asymptotically, and the convergence time is related to the selected control gain. Secondly, the system is mainly affected by the switching signal ($sign^*$) and various motion delays, which makes it easy to generate undesirable chattering. Many solutions have been proposed to eliminate the above disadvantages. A nonlinear switching surface was designed to ensure the finite-time convergence [25]. A novel, nonsingular, fast terminal sliding mode controller using terminal sliding mode control technology to solve the fast finite-time control problem of the dynamic system was proposed in [26]. A new adaptive exponential reaching law (ERL) was proposed in [27], which overcomes the limitation of ERL, reduces chattering and improves convergence speed. Based on the power reaching law and constant reaching law, a novel strategy for the vertical motion control of the designed AUV is proposed, which can improve the convergence speed and increase the dynamic performance of the system. The horizontal motion is not as complex as the vertical motion, so the S-plane controller [28] with a simple structure and fewer parameters is applied in the horizontal motion.

The rest of the paper is organized as follows. Section 2 describes the plateau data-gathering AUV's hardware and software. In Section 3, the control strategies are described. A novel sliding mode controller was designed, and four vertical thrusters were equipped to increase the accuracy and efficiency of the vertical hovering control. In Section 4, the simulation of vertical motions compared with conventional sliding mode control was performed to demonstrate the feasibility of the controller. Experiments in the tank and the plateau river were performed to verify the feasibility and reliability of the AUV. Finally, a short conclusion and future works are given in Section 5.

2. Design of the AUV Platform

The AUV (Figure 1) consists of a carbon fiber shroud, a pressure shell, and communication, propulsion, and electronic control systems. The major parameters are presented in Table 1. The AUV is equipped with various sensors, such as a Doppler Velocity Log (DVL, LinkQuest Inc., San Diego,

California, USA), a depth sensor (Valeport Ltd., Totnes, Devon, UK), an Acoustic Doppler Current Profiler (ADCP, Rowe Technologies Inc., Powayd, CA, USA), and a water quality sensor (Valeport Ltd., Totnes, Devon, UK). Its actuator is composed of two horizontal thrusters and four vertical thrusters. To improve navigational stability, an X-wing stabilizer was added to the stern housing.

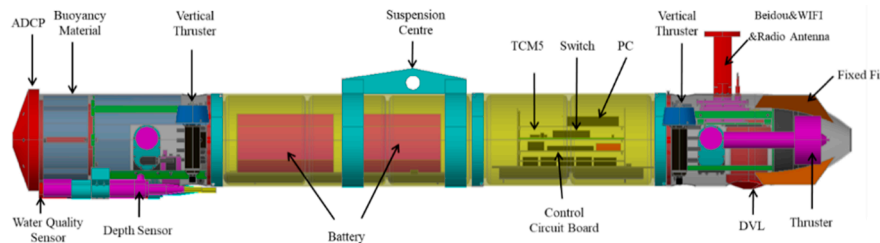


Figure 1. Plateau data-gathering AUV (autonomous underwater vehicle).

Table 1. Key specifications of the AUV.

Length	96 kg
Width	0.5 m
Maximum Diameter	0.28 m
Height	0.47 m
Maximum Depth	100 m
Cruising Speed	4 km
Actuators	two horizontal thrusters, four vertical thrusters
Communication Equipment	BeiDou+GPS, radio, Wi-Fi
Sensors	TCM5, depth sensor, DVL, water quality sensor, ADCP

The AUV can be divided into the following parts.

- 1) The structure includes the pressure and non-pressure shells and the connecting frame. The pressure shell is made of non-magnetic, corrosion-resistant, lightweight, and high-strength aluminum alloy. The connecting frame is made of aluminum alloy and polypropylene. The non-pressure shell is made of high-strength carbon fiber.
- 2) The propulsion and maneuvering system consists of two horizontal and four vertical thrusters, which control surge velocity, heading, depth, and pitch.
- 3) Energy is provided by two rechargeable lithium batteries: a 7 S 80Ah control system battery and a 13 S 40 Ah power system battery.
- 4) The navigation and positioning system consists of a transcutaneous monitor (TCM) 5, a DVL, a depth sensor, and BeiDou.

2.1. Design of the Control System

The AUV system consists of the ground station and AUV (Figure 2). The ground station and the AUV communicate via BeiDou, radio, and Wi-Fi. Control and status commands are sent and received via BeiDou and radio, whereas data and program updates are uploaded and downloaded via Wi-Fi. The hardware architecture of the plateau data-gathering AUV system is presented in Figure 3.



Figure 2. Plateau data-gathering AUV system (left: developed AUV; right: ground station).

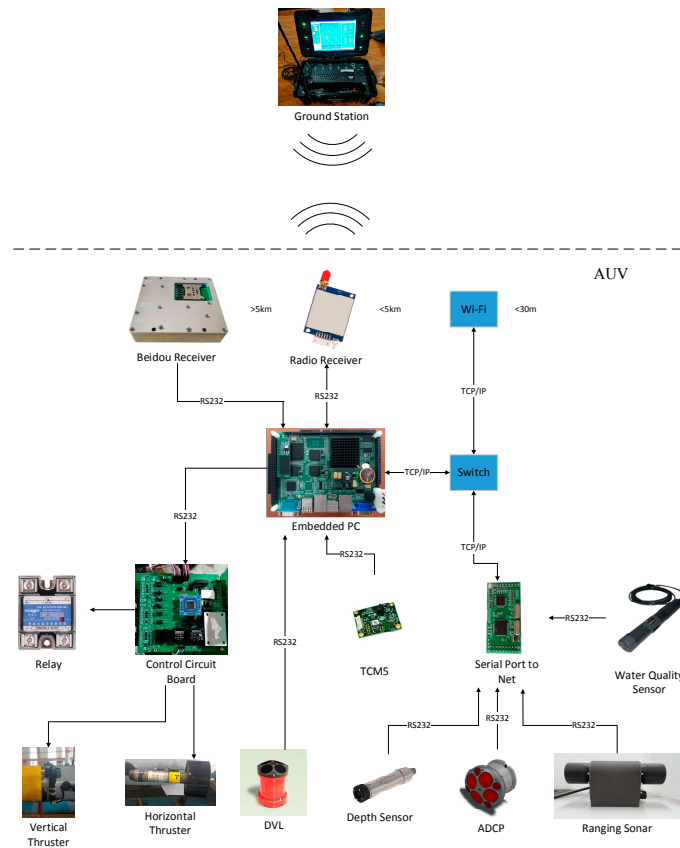


Figure 3. Hardware architecture of the AUV.

The underwater control system of the plateau data-gathering AUV consists of a low-power embedded computer equipped with a VxWorks system, switches, and communication antenna, among others. The computer has a rich interface to connect various sensors and devices. The radio, BeiDou positioning and communication, DVL, TCM5 and ADCP are connected via RS232 serial ports. The sensors' accuracy is presented in Table 2.

Table 2. Specifications of the applied sensors.

Sensors	Items	Accuracy
TCM5	Heading accuracy	0.3°
	Pitch-and-roll accuracy	0.2°
DVL	Maximum velocity	±20 knots
	Velocity accuracy	0.2% ± 1 mm/s
	Accuracy	±0.01% FS
Depth sensor	Temperature accuracy	±0.05 °C
	Conductivity accuracy	±0.05 ms/cm
	Salinity accuracy	±0.05 ppt
Water quality sensor	Dissolved oxygen accuracy	±0.5%
	Turbidity accuracy	±0.5 ntu(0–300ntu) ±5 ntu(300–600ntu)
	pH accuracy	±0.03

The plateau data-gathering AUV actuator consists of two horizontal thrusters and four vertical thrusters. To evaluate the propulsion performance of the thrusters and improve control precision, a series of open water experiments were conducted in a water tank to obtain the thrust performance curve (Figure 4). Some of the thrust curves are presented in Figure 5. In particular, the left illustrates the left horizontal thruster thrust curve, whereas the other illustrates the right horizontal thruster thrust curve.



Figure 4. Testing of thrusters (left: fixing method; right: testing with current).

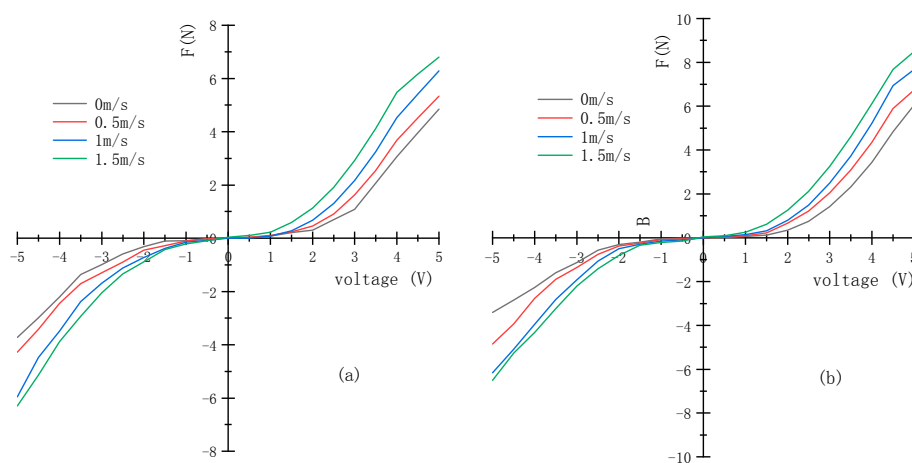


Figure 5. Thrust curves of some thrusters at different currents. (a): the left horizontal thruster thrust curve. (b): the right horizontal thruster thrust curve.

2.2. Software Architecture of the AUV

The core of the plateau data-gathering AUV ground station is a high-performance computer. The monitoring software is compiled by VC++6.0 (Microsoft, Redmond, Wash., USA). The monitoring software not only displays sensor information, such as display attitude, speed, altitude, battery voltage, and current, but also controls the switch of the AUV sensor, loads the map of local waters, and generates and sends path points.

The underwater system software is divided into three parts: the basic control, navigation, and path-tracking modules. The logical structure diagram of the underwater system software is presented in Figure 6. The system processes the command that is received from the ground station. It determines if the current task state is either basic control or planning control, and then executes the corresponding program in accordance with different states.

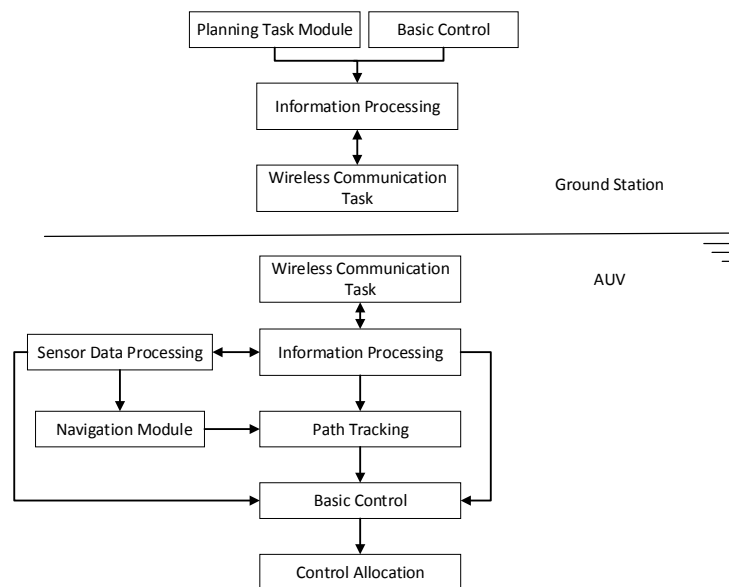


Figure 6. Logic structure diagram of AUV software system.

3. Control Strategies for the Developed AUV

3.1. Dynamic Equations of Motion

The AUV’s corresponding coordinate systems are shown in Figure 7. For convenience in investigating the AUV, we establish an inertial reference frame $E - \xi\eta\zeta$ and a body-fixed frame $O - xyz$. The original point of the inertial reference frame can be set at any place in the ocean, and the original point is usually set at the AUV’s gravity center. The definitions of the parameter are shown in Table 3.

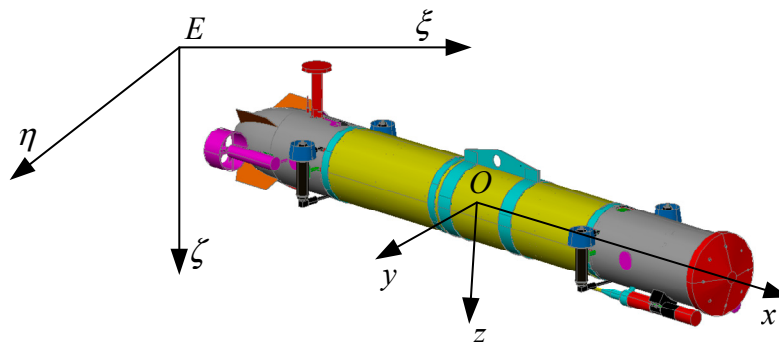


Figure 7. Body-fixed frame and inertial reference frame.

Table 3. The parameters of AUV’s motion.

DOF	Forces and Moments	Linear and Angular Velocities	Positions and Euler Angles
Surge	X	u	x
Sway	Y	v	y
Heave	Z	w	z
Roll	K	p	ϕ
Pitch	M	q	θ
yaw	N	r	ψ

According to reference [29], the 6-DOF nonlinear equations of motion can be written as:

$$\dot{\eta} = J(\eta)v \tag{1}$$

$$Mv + C(v)v + D(v)v + g(\eta) = \tau \tag{2}$$

where η denotes the position and orientation vector with coordinates in the earth fixed frame, $J(\eta)$ is the transform matrix between the body-fixed and inertial coordinates, v denotes the linear and angular velocity vector with coordinates in the body-fixed frame, M is the inertial and add inertial matrix, $C(v)$ is the matrix of Coriolis and Centrifugal terms, $D(v)$ is the matrix of hydrodynamics terms, $g(\eta)$ is the vector of gravity and buoyant force, τ denotes the forces and moments in the body-fixed frame.

$$\eta = (x, y, z, \phi, \theta, \psi)^T \tag{3}$$

$$J(\eta) = \begin{bmatrix} J_1(\eta) & 0_{3 \times 3} \\ 0_{3 \times 3} & J_2(\eta) \end{bmatrix} \tag{4}$$

$$J_1(\eta) = \begin{bmatrix} c\psi c\theta & c\psi s\theta s\phi - s\phi c\psi & s\phi s\psi + c\psi s\theta c\phi \\ s\theta s\phi & s\phi s\theta s - c\phi c\psi & s\psi s\theta c\phi - c\psi s\phi \\ -s\theta & c\theta s\phi & c\theta c\phi \end{bmatrix} \tag{5}$$

$$J_2(\eta) = \begin{bmatrix} 1 & s\phi t\theta & c\phi t\theta \\ 0 & c\phi & -s\phi \\ 0 & s\phi/c\theta & c\phi/c\theta \end{bmatrix} \tag{6}$$

$$M = \text{diag}\{m - X_{\dot{u}}, m - Y_{\dot{v}}, m - Z_{\dot{w}}, I_{xx} - K_{\dot{p}}, I_{yy} - M_{\dot{q}}, I_{zz} - N_{\dot{r}}\} \tag{7}$$

$$C(v) = \begin{bmatrix} 0_{3 \times 3} & C_1 \\ -C_1^T & C_2 \end{bmatrix} \tag{8}$$

$$C_1 = \begin{bmatrix} 0 & (m_{33} - Z_{\dot{w}})w_r & -(m_{22} - Y_{\dot{v}})v_r \\ -(m_{33} - Z_{\dot{w}})w_r & 0 & (m_{11} - X_{\dot{u}})u_r \\ (m_{22} - Y_{\dot{v}})v_r & -(m_{11} - X_{\dot{u}})u_r & 0 \end{bmatrix} \tag{9}$$

$$C_2 = \begin{bmatrix} 0 & (I_{zz} - N_{\dot{r}})r & -(I_{yy} - M_{\dot{q}})q \\ -(I_{zz} - N_{\dot{r}})r & 0 & (I_{xx} - K_{\dot{p}})p \\ (I_{yy} - M_{\dot{q}})q & -(I_{xx} - K_{\dot{p}})p & 0 \end{bmatrix} \tag{10}$$

$$D(v) = -\text{diag}\{X_{\dot{u}} + X_{|u|}|u|, Y_{\dot{v}} + Y_{|v|}|v|, Z_{\dot{w}} + Z_{|w|}|w|, K_p + K_{p|p|}|p|, M_q + M_{q|q|}|q|, N_r + N_{r|r}|r|\} \tag{11}$$

$$g(\eta) = \begin{bmatrix} (W - B)s\theta \\ -(W - B)c\theta s\psi \\ -(W - B)c\theta c\psi \\ y_B Bc\theta c\psi - z_B Bc\theta s\psi \\ -z_B Bs\theta - x_B Bc\theta c\psi \\ x_B Bc\theta s\psi + y_B Bs\theta \end{bmatrix} \quad (12)$$

$$\tau = [X, 0, Z, 0, M, N]^T \quad (13)$$

where W and B denote the gravity and buoyancy of the AUV, (x_B, y_B, z_B) is the coordinate of floating center, c , s and t are shorthand for the mathematical expression of \cos , \sin , and \tan , respectively.

3.2. Design of Path Tracking

Path tracking is not subject to time constraints and only requires the AUV to converge on the desired path. A line-of-sight (LOS) algorithm is used as a guiding strategy. The principle is independent of dynamic control and models and requires few parameters to be designed. The desired heading is only related to the AUV's real-time position and expected route. By providing a series of path points $[x_d(k), y_d(k)], k = 1, 2, \dots, N$, the AUV travels to each path point in turn (Figure 8). The heading angle of the AUV can be defined as:

$$\psi_d(t) = \arctan \frac{y_d(k) - y(t)}{x_d(k) - x(t)} \quad (14)$$

The safety radius ρ is set to the center of each path point. If the AUV enters the safe radius, then it is considered to reach this point and will sail toward the next point. The arrival condition is determined as:

$$\sqrt{(x_d(k) - x(t))^2 + (y_d(k) - y(t))^2} \leq \rho \quad (15)$$

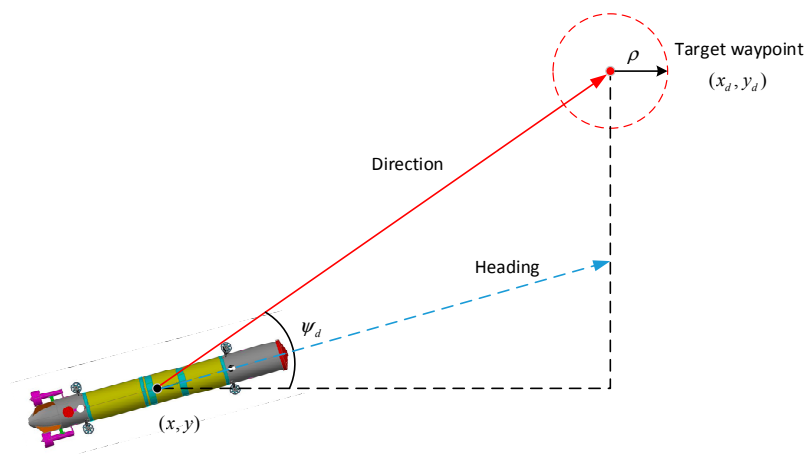


Figure 8. Waypoint tracking with heading control of the AUV.

3.3. Design of Navigation Strategy

The navigation mode of the plateau data-gathering AUV combines dead reckoning and BeiDou (Figure 9). The logic diagram of the integrated navigation algorithm is presented in Figure 9. When the AUV navigates underwater, the dead-reckoning algorithm is applied. The flowchart of the dead-reckoning algorithm is presented in Figure 10. Speed information is provided by the DVL. The horizontal position change of the AUV is obtained by integrating the velocity after processing. The 3D position of the AUV is determined by considering the initial position and depth sensor information. The deviation between the position calculated via dead reckoning and the actual position of the AUV increases with time [30] because of the error and integral error of the sensor. To eliminate this deviation,

the AUV uses BeiDou positioning information for position correction. If the BeiDou information is invalid, then the data information is disregarded, and the position information calculated via dead reckoning is used. If the information is valid, then the BeiDou position data and the dead reckoning result are combined using the Kalman algorithm.

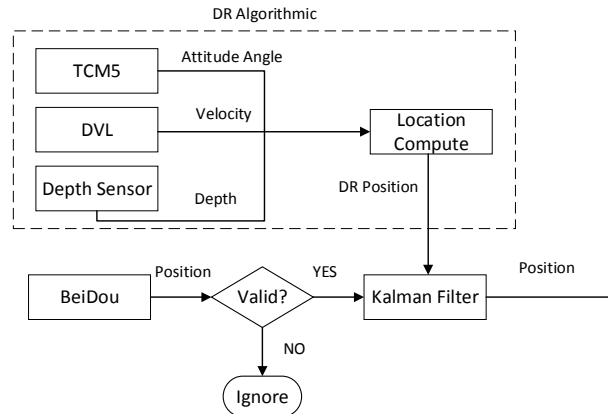


Figure 9. Logic diagram of navigation algorithm.

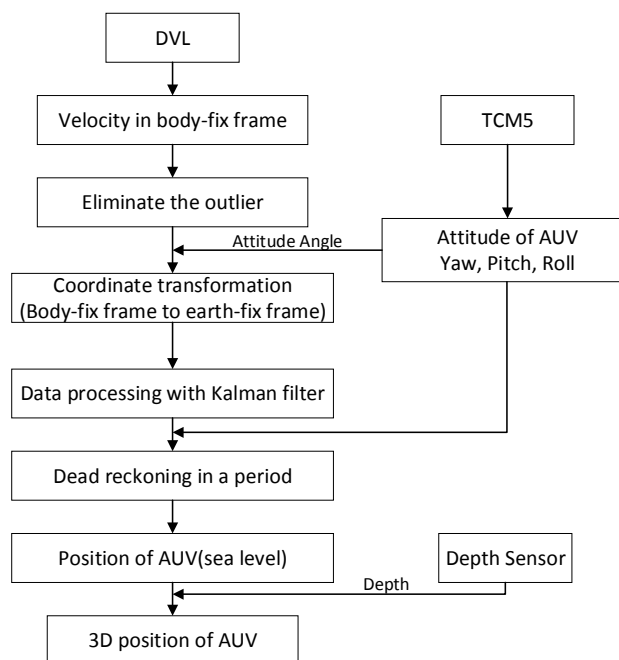


Figure 10. Dead-reckoning algorithm.

3.4. Controllers Design

As mentioned in the introduction, the vertical motion is much more complicated than the horizontal motion. A novel sliding mode controller is designed for the vertical motion control, while a controller with a simple structure and few parameters is adopted for the horizontal motion control.

3.4.1. Sliding Mode Controller Design

AUVs are strong coupling and highly nonlinear systems typically, and it is difficult to establish accurate motion models. Among the various AUV control algorithms, the sliding mode controlled by sliding mode variable structure is robust to parameter changing and unmodeled parts of the system, which makes the SMC method an effective method for controlling AUVs [31–33] In summary,

considering the complexity of vertical motions of the AUV, the SMC method is chosen as a controller for vertical motion.

A novel adaptive combined sliding mode reaching law based on the power rate reaching law and constant reaching law is proposed to improve dynamic performance and robustness.

The adaptive combined reaching law can be written as:

$$\dot{s} = -k_1 |s|^\alpha \operatorname{sgn}(s) - \chi \operatorname{sgn}(s) \tag{16}$$

where, $k_1 > 0, \alpha > 0, \lambda > 0, \mu > 0, \chi = \frac{\lambda}{\mu + (1-\mu)e^{-k_2|s|}}$. It can be seen that $\chi > 0$, and the proposed reaching law does not affect the system stability. When $|s|$ increases, χ tends to λ/μ , the power rate reaching law will play the major role so that the reaching speed is large enough. When $|s|$ decreases, $-k_1 |s|^\alpha \operatorname{sgn}(s)$ tends to 0, the effect of power rate reaching law is reduced, χ tends to λ . While approaching to the sliding surface, χ decreases, it can weaken the effects of buffeting.

Stability analyze:

Theorem 1. *The adaptive approach law satisfies the arrival condition.*

Proof. Choose the Lyapunov function as $V = \frac{1}{2}s^2$, and deriving it we get $\dot{V} = -k_1 |s|^{\alpha+1} - \chi |s|$. As $k_1 > 0, \chi > 0$, we can yield $\dot{V} < 0$. □

Theorem 2. *The system can reach the sliding surface in a finite time.*

Proof. We assumed initial condition $s(0) > 1$, the provident of the reaching time is divided in two stages.

Stage 1 S tends from the initial position $s(0)$ to 1. In this stage, $-k_1 |s|^\alpha \operatorname{sgn}(s) \gg -\chi \operatorname{sgn}(s)$, ignore the impact of $-\chi \operatorname{sgn}(s)$ can be ignored, we can get

$$ds/dt = -k_1 s^\alpha \tag{17}$$

Set the final stable time as t_1 and integrate it

$$t_1 = [1 - s(0)^{1-\alpha}] / [k_1(\alpha - 1)] \tag{18}$$

Stage 2 S tends from 1 to 0. In this stage, $-\chi \operatorname{sgn}(s) \gg -k_1 |s|^\alpha \operatorname{sgn}(s)$, ignore the impact of $-k_1 |s|^\alpha \operatorname{sgn}(s)$, we get

$$ds/dt = \frac{\lambda}{\mu + (1-\mu)e^{-k_2|s|}} \operatorname{sgn}(s) \tag{19}$$

Set the final stable time as t_2 and integrate it

$$t_2 = \frac{1}{\lambda} (\mu |s(0)| + (1-\mu) \int_0^{s(0)} \operatorname{sign}(s) e^{-k_2|s|} ds) \tag{20}$$

If $s \leq 0$ for all $t \leq t_2$:

$$\int_0^{s(0)} \operatorname{sign}(s) e^{-k_2|s|} ds = - \int_0^{s(0)} e^{-k_2|s|} ds = \int_0^{-s(0)} e^{-k_2|s|} ds \tag{21}$$

If $s \geq 0$ for all $t \leq t_2$:

$$\int_0^{s(0)} \text{sign}(s)e^{-k_2|s|} ds = \int_0^{s(0)} e^{-k_2|s|} ds \tag{22}$$

According to (21) and (22), (20) can be rewritten as:

$$\begin{aligned} t_2 &= \frac{1}{\lambda}(\mu|s(0)|) + (1-\mu) \int_0^{|s(0)|} e^{-k_2|s|} ds \\ &= \frac{1}{\lambda}(\mu|s(0)|) + \frac{(1-\mu)}{k_2}(1 - e^{-k_2|s(0)|}) \end{aligned} \tag{23}$$

Therefore, the total time that the system state reaches the sliding surface is

$$t = t_1 + t_2 = \frac{1-s(0)^{1-\alpha}}{k_1(\alpha-1)} + \frac{1}{\lambda}(\mu|s(0)|) + \frac{(1-\mu)}{k_2}(1 - e^{-k_2|s(0)|}) \tag{24}$$

Hence, system can reach the sliding surface in finite time. □

According (1) and (2), the model of AUV can be written as

$$\dot{x} = Ax + Bu + d \tag{25}$$

where $x = [z \ \theta \ w \ q]^T$, $A = H^{-1}P$, $B = H^{-1}$

$$H = \begin{bmatrix} 1 & 0 & 0 & 0 \\ 0 & 1 & 0 & 0 \\ 0 & 0 & m_{11} - X_{\dot{u}} & -(mx_g + z_{\dot{q}}) \\ 0 & 0 & -(mx_g + M_{\dot{w}}) & I_{yy} - M_{\dot{q}} \end{bmatrix}, P = \begin{bmatrix} 0 & -U & 1 & 0 \\ 0 & 0 & 0 & 1 \\ 0 & 0 & Z_w & mU + Z_q \\ 0 & M_{\theta} & M_w & -mx_g U + M_q \end{bmatrix}, U \text{ denote the surge velocity.}$$

Sliding surface can be defined as follows

$$s = C\tilde{x} \tag{26}$$

where $\tilde{x} = x - x_d$ are state errors, x_d is desired state.

Then derivate s , we get

$$\dot{s} = C(\dot{x} - \dot{x}_d) = C(Ax + Bu + d - \dot{x}_d) \tag{27}$$

Substitute (16) into the above equation, we can yield:

$$\dot{s} = C(Ax + Bu + d - \dot{x}_d) = -k_1|s|^\alpha \text{sgn}(s) - \chi \text{sgn}(s) \tag{28}$$

The control input u from (28) can be extracted as

$$u = (CB)^{-1}[C\dot{x}_d - CAx - Cd - k_1|s|^\alpha \text{sgn}(s) - \chi \text{sgn}(s)] \tag{29}$$

Considering the problem of chattering in sliding mode control, boundary layer processing method is used. $\text{sat}(\cdot)$ is the processed switching control, which can be expressed as

$$\text{sat}(s) = \begin{cases} 1 & s > \Delta \\ \frac{s}{\Delta} & -\Delta \leq s \leq \Delta \\ -1 & s < -\Delta \end{cases} \tag{30}$$

The control law can be rewritten as:

$$u = (CB)^{-1} [C\dot{x}_d - CAx - Cd - k_1|s|^\alpha \text{sat}(s) - \chi \text{sat}(s)] \tag{31}$$

3.4.2. S-Plane Controller

The control algorithm of horizontal motion for the plateau data-gathering AUV uses the S-plane control algorithm [28]. The method combines the fuzzy control concept and the proportional-integral-derivative control structure, which has the advantages of a simple structure and few parameters. The method has been successfully applied to the motion control of multi-type underwater vehicles and has achieved satisfactory control effects.

The S-plane control algorithm is as follows:

$$\begin{cases} u_i = \frac{2.0}{1.0 + \exp(-k_{i1}e_i - k_{i2}\dot{e}_i)} - 1.0 + \Delta u_i \\ f_i = K_i u_i \end{cases} \tag{32}$$

where u_i is the output of the i degree of freedom control, e_i and \dot{e}_i denote the input information of the i degree of freedom control (deviation and deviation rate after normalization). k_{i1} and k_{i2} indicate the control parameters that correspond to the degree of freedom, deviation, and deviation rate. The control effect can be adjusted by changing the value of the parameters, where f_i is the force/moment required for the degree of freedom, K_i is the maximum force/moment provided in the degree of freedom, and Δu_i is an adjustment item for adapting to environmental interference.

The control of the plateau data-gathering AUV is divided into two control channels: surge velocity, and heading. The control parameters of each channel controller are presented in Table 4.

Table 4. Controller parameters.

	k_1	k_2
Surge velocity control	0.6	0.2
Heading control	0.05	0.1

3.5. Control Allocation

The plateau data-gathering AUV has a slender body. The actuator consists of six thrusters: two horizontal thrusters and four vertical thrusters. The arrangement of the thrusters on the AUV is shown in Figure 11, where l_1, l_2, l_3 and l_4 are the arms of force of each thruster.

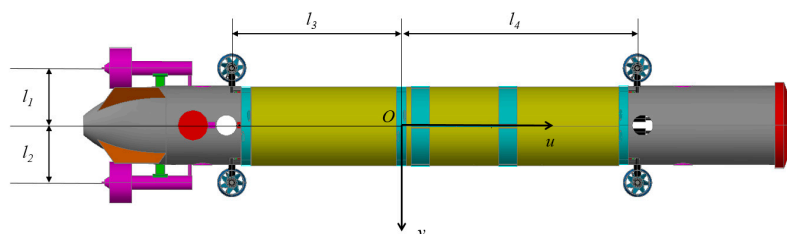


Figure 11. Layout of the AUV thrusters.

The relationship between the required moment and the force generated by the thrusters is:

$$\begin{bmatrix} X \\ Z \\ M \\ N \end{bmatrix} = \begin{bmatrix} 1 & 1 & 0 & 0 \\ 0 & 0 & 1 & 1 \\ 0 & 0 & l_3 & -l_4 \\ l_1 & -l_2 & 0 & 0 \end{bmatrix} \begin{bmatrix} T_1 \\ T_2 \\ T_3 + T_4 \\ T_5 + T_6 \end{bmatrix} \tag{33}$$

where X , Z , M , and N are the longitudinal force, vertical force, pitching moment, and shaking moment, respectively; T_1 and T_2 are the thrusts of the left and right horizontal thrusters; and T_3, T_4, T_5 , and T_6 are the thrusts of the SL, SR, BR, and BL vertical thrusters, respectively.

The plateau data-gathering AUV adopts the principle of swaying and trimming priority for control allocation. In the actual process, the thrusters have a maximum thrust limit T_{max} . If the thrust of a propeller is calculated to be greater than T_{max} , then the priority principle should be used for allocation.

If the horizontal or vertical thrusters have only one thruster with a side (left or right, and bow or stern) thrust greater than T_{max} , then:

$$\begin{cases} T_1 = T_{max} \\ T_2 = \frac{T_{max}l_1 - N}{l_1 + l_2} \end{cases} \quad (34)$$

$$\begin{cases} T_3 = T_4 = T_{max} \\ T_5 = T_6 = \frac{T_{max}l_3 - M}{l_3 + l_4} \end{cases} \quad (35)$$

If $|T_2| > T_{max}$ or $|T_5| = |T_6| > T_{max}$, then in the same manner, $|T_2| = T_{max}, |T_5| = |T_6| = T_{max}$.

4. Simulations and Experiments

The proposed adaptive reaching law of vertical motion is verified in Matlab-Simulink and compared with the conventional sliding mode control and the PID controller. The extra force and moment generated by the antenna is considered in the simulation process. The simulation results are shown in Figures 12 and 13.

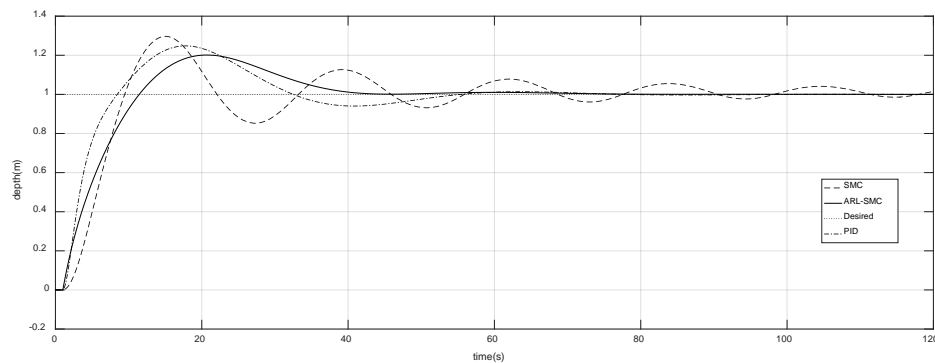


Figure 12. Depth response curves of simulation.

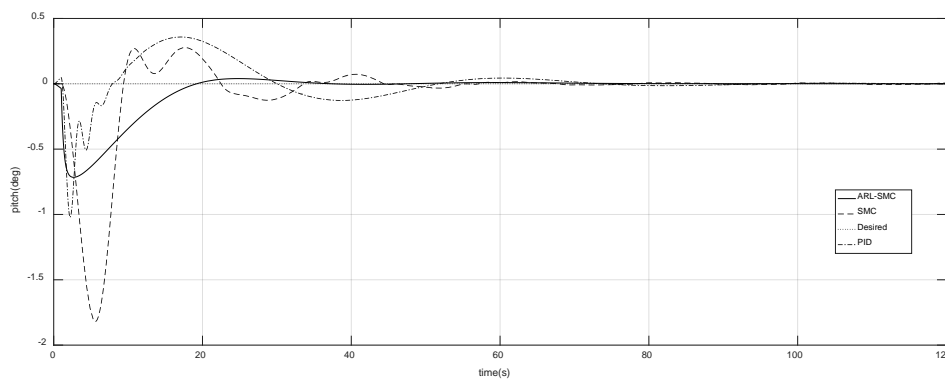


Figure 13. Pitch response curves of simulation.

It can be seen from the simulation results that the depth and pitch angle of AUV will be shaken with the conventional SMC due to the presence of the external disturbances. This jitter takes a long time to eliminate. The SMC of adaptive combined sliding mode reaching law has faster convergence

speed and smaller overshoot than conventional SMC and PID, which can eliminate the interference of external disturbance to the system and achieve the stability of depth control.

Relevant field experiments were conducted to verify the reliability and stability of the entire plateau data-gathering AUV system.

In the tank of the Science and Technology on Underwater Vehicle Laboratory in Harbin Engineering University, basic navigation verifications, such as depth, heading, and surge velocity controls, were conducted. In addition, functional verification tests were performed in Longyangxia in Qinghai Province, China. The experiment sites are shown in Figure 14.



Figure 14. Experiment sites in the tank (left) and on the Tibetan Plateau (right).

The heading control experiment is presented in Figure 15. The red dotted line indicates the target heading. In this experiment, the target heading is 0 , 250° , and -250° . When the AUV is in the direction of the given target, no other action is performed. As shown in the figure, the AUV achieves satisfactory heading control, can reach the target heading in the vicinity, and stabilizes quickly. The results of the depth control experiment are presented in Figure 16, and the results of the automatic speed control experiment are presented in Figure 17. The figures showed that depth and velocity controls achieve satisfactory effects and meet the basic detection requirements. The results of hovering control are shown in Figure 18. The initial depth (0.5 m) and pitch (0°) were kept static in 152 beats. After that, the AUV was commanded to track the desired depth of 1.15 m in 338 beats. At 490 beats, hovering motion control was stopped, and the maximum pitch angle is -17° . The experiment results showed that the errors of depth and pitch angle are within a small range with the control of the controller.

The result of the comprehensive experiment is presented in Figure 19. The experiment was conducted in parallel with velocity, heading, and depth. Simultaneous depth, direction, and speed controls were performed at 132–480, 550–1020, 1226–1690, and 1830–2800 beats. The control effect is good, reaches the target command, and stabilizes in time. The fixed-point control experiment was conducted at 1020–1226 beats. During this moment, the target speed was 0 , the target direction was -169° , and the target depth was 0.3 m. The fixed-point control effect is very good for speed, direction, and depth. All are stable near the target command. Depth was not controlled at 1828–2460 beats. The AUV performed at constant speed and orientation tests on the water surface. At the 2460th beat, the target depth became 0.9 m, the heading remained stable near the target, but velocity was affected, thereby resulting in deceleration. When the target depth was reached, velocity gradually stabilized. The AUV was affected by the controlled allocation strategy when diving. The stern entered the water first, and the attitude change increased longitudinal resistance, thereby reducing speed. The experiment results show that depth, speed, and direction are effectively controlled, which meets the requirements for river detection tasks.

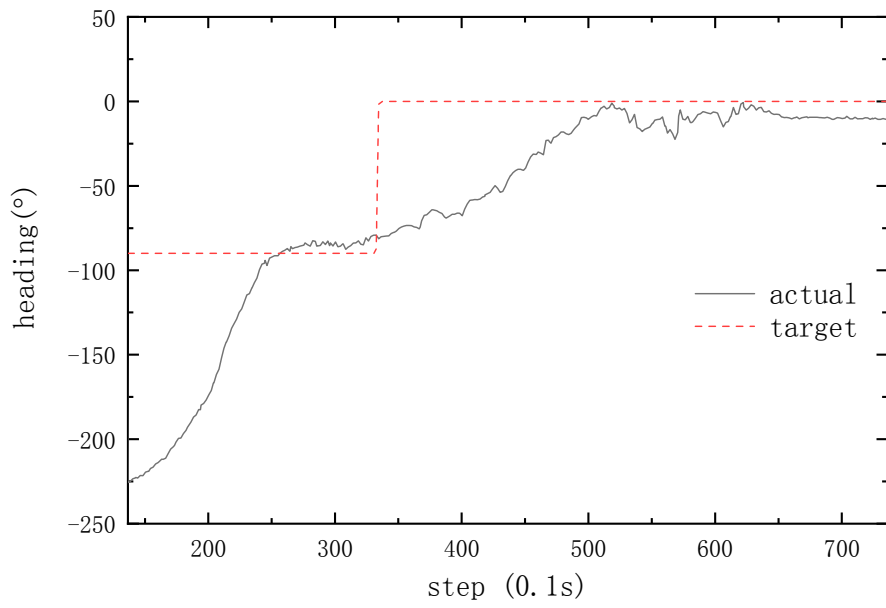


Figure 15. Automatic control of the heading.

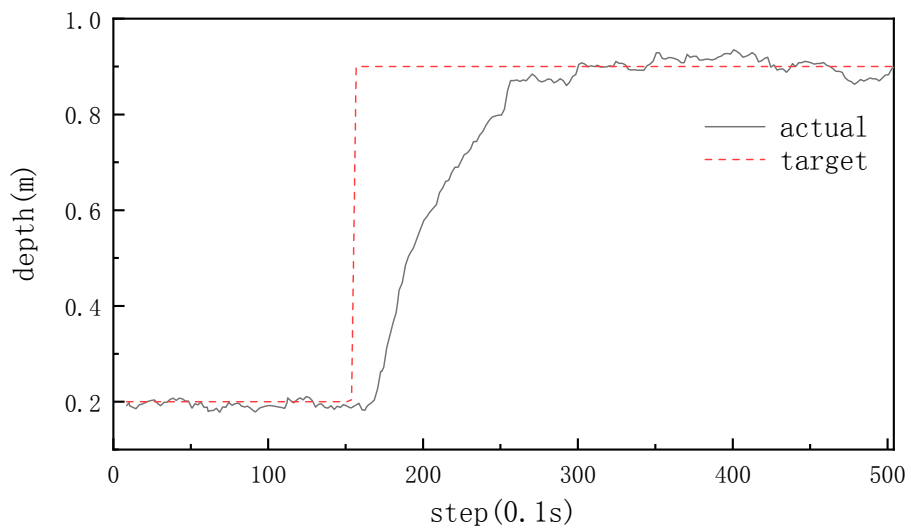


Figure 16. Automatic control of the depth.

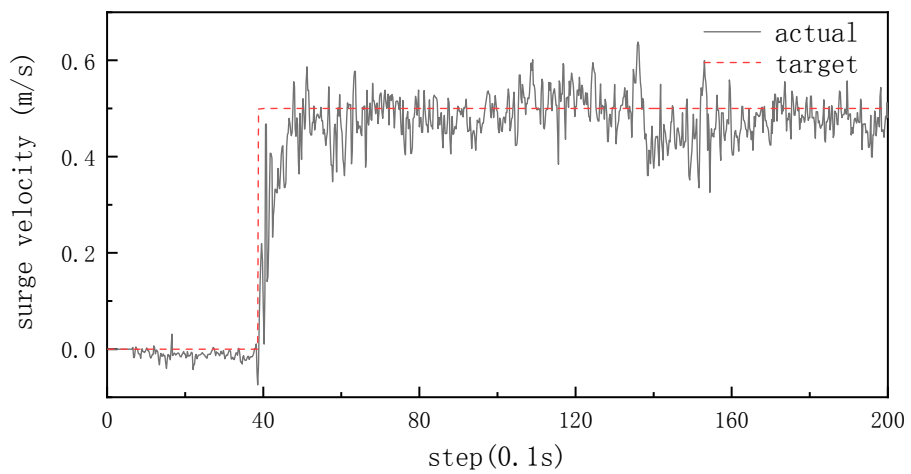


Figure 17. Automatic control of the velocity.

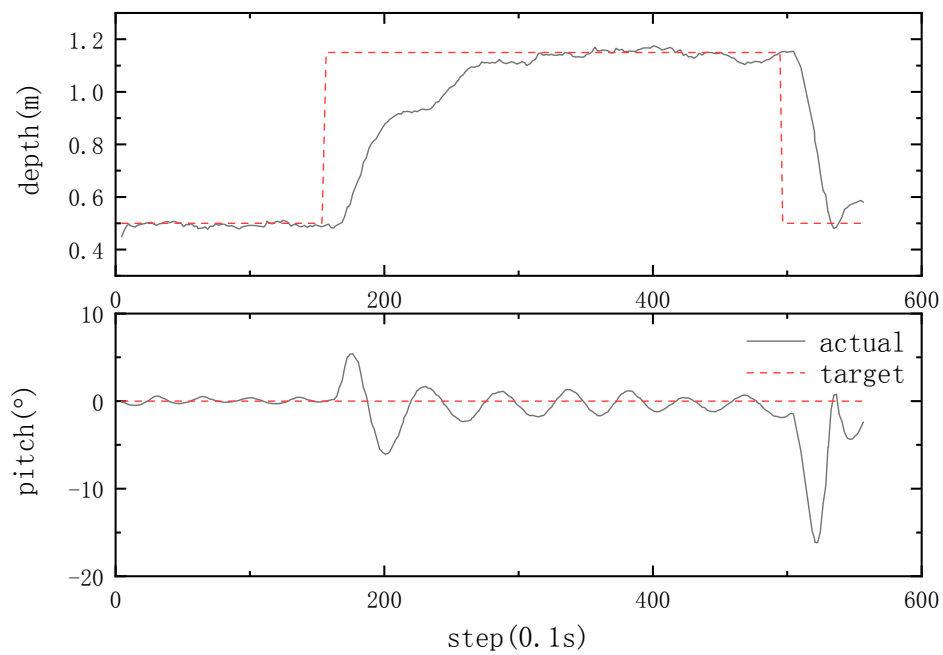


Figure 18. Vertical plane motion automatic control.

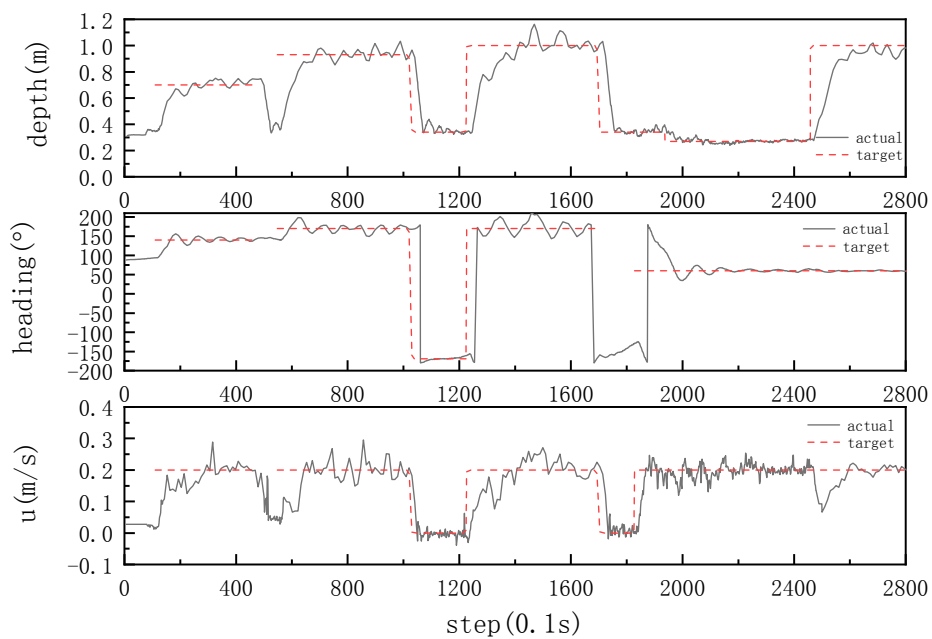


Figure 19. Experimental result of automatic control.

Figure 20 presents the result of the plateau river experiment conducted in Longyangxia, Qinghai. The red dotted line is the desired path, whereas the black solid line is the actual path. As illustrated in the figure, the AUV can effectively track the target path.

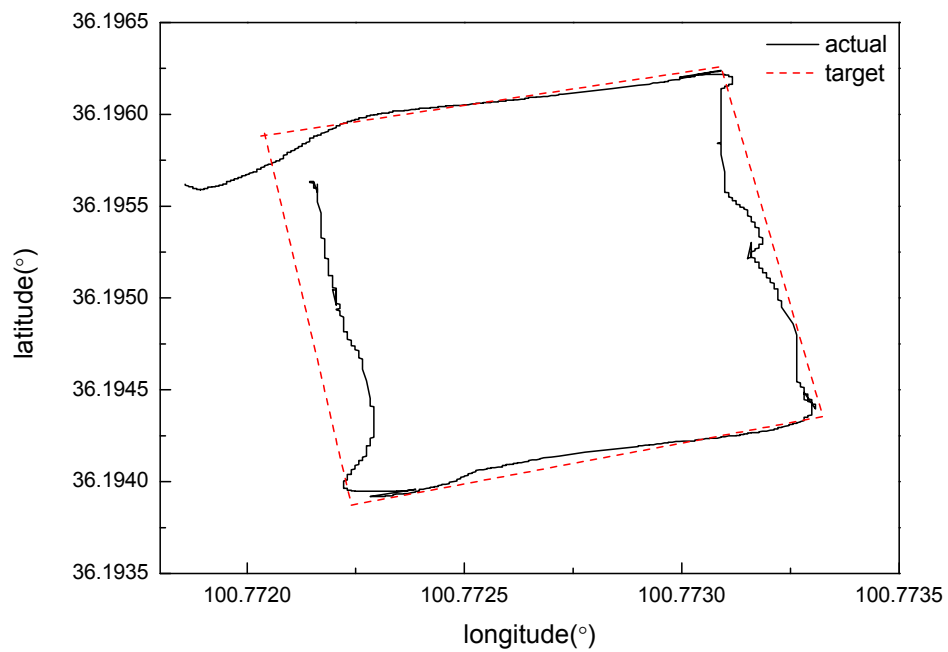


Figure 20. Experimental result of path tracking.

The AUV collected the hydrological conditions of the Longyangxia area using the water quality sensor. Partial results of the detection are presented in Figure 21, including the water depth map (a), the oxidation–reduction potential distribution (b), and the pH level (c). The value distribution map and the diagram (d) are the dissolved oxygen (DO%) distribution maps.

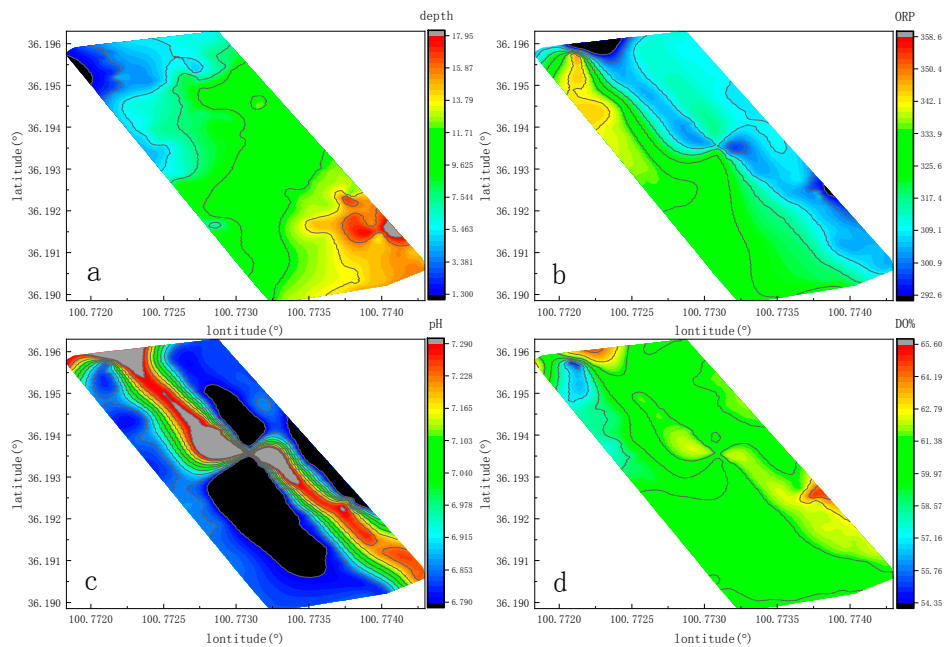


Figure 21. Partial hydrological results. (a): Depth of the detecting water; (b): Oxidation reduction potential distribution (ORP) of the detecting water; (c): pH value of the detecting water; (d): Dissolved oxygen (DO%) of the detecting water.

5. Conclusions

In this paper, the design, control, and implementation of a plateau data-gathering AUV platform are presented. With two horizontal thrusters and four vertical thrusters, the hovering and maneuverability of this vehicle are excellent.

The control system, including hardware composition and software structure, is designed. The navigation system adopts the integrated navigation method of TCM5–DVL–BeiDou based on the Kalman filter. Tracking control adopts the tracking control strategy based on the LOS method. A novel sliding mode controller based on adaptive reaching law for vertical motion control (ARL-SMC) is proposed, while the S-plane controller is used for horizontal motion. Results of vertical motion simulation show that the proposed controller results in shorter convergence time and gets smaller overshoot than the conventional sliding mode controller. Finally, the results of tank and field experiments demonstrate the feasibility and reliability of the AUV control system.

In the subsequent research, the situation of thrusters' saturation and failure will be considered in the controller design. Optimal control considering energy consumption will be studied to increase the endurance.

Author Contributions: Conceptualization, H.X. and G.-C.Z.; Methodology, H.X., G.-C.Z. and Y.-S.S.; Software, X.W., X.-R.R. and H.X.; Investigation, H.X. and X.-B.W.; Resources, S.P. and Y.-S.S.; Writing—original draft preparation, H.X.; Writing—review and editing, H.X., X.-B.W. and X.-R.R.; Supervision, Y.-S.S. and S.P.; Project administration, Y.-S.S.; Funding acquisition, Y.-S.S. The final manuscript has been approved by all the authors.

Funding: This research was part of the project (Grant No. 41412030201) supported by Equipment Pre-Research Project. It has also been partially supported by Natural Science Foundation of China (Grant No. 51779057, 51709061, 51609047). Great thanks are addressed to them by the research team.

Acknowledgments: The author would like to thank the reviewers for their comments on improving the quality of the paper. Special thanks also go to the employees of Harbin Engineering University for their assistance during the field experiments.

Conflicts of Interest: The authors declare no conflict of interest.

References

- Cheng, G.; Jin, H. Permafrost and groundwater on the Qinghai-Tibet Plateau and in northeast China. *Hydrogeol. J.* **2013**, *21*, 5–23. [[CrossRef](#)]
- Pennington, J.T.; Blum, M.; Chavez, F.P. Seawater sampling by an autonomous underwater vehicle: “Gulper” sample validation for nitrate, chlorophyll, phytoplankton, and primary production. *Limnol. Oceanogr. Methods* **2016**, *14*, 14–23. [[CrossRef](#)]
- Xiang, X.; Lapierre, L.; Jouvencel, B. Smooth transition of AUV motion control: From fully-actuated to under-actuated configuration. *Robot. Auton. Syst.* **2015**, *67*, 14–22. [[CrossRef](#)]
- Yu, C.; Xiang, X.; Lapierre, L.; Qin, Z. Robust Magnetic Tracking of Subsea Cable by AUV in the Presence of Sensor Noise and Ocean Currents. *IEEE J. Ocean. Eng.* **2017**, *43*, 311–322. [[CrossRef](#)]
- Huang, S.W.; Chen, E.; Guo, J. Efficient Seafloor Classification and Submarine Cable Route Design Using an Autonomous Underwater Vehicle. *IEEE J. Ocean. Eng.* **2017**, *43*, 7–18. [[CrossRef](#)]
- Xiang, X.; Jouvencel, B.; Parodi, O. Coordinated Formation Control of Multiple Autonomous Underwater Vehicles for Pipeline Inspection. *Int. J. Adv. Robot. Syst.* **2010**, *7*, 3. [[CrossRef](#)]
- Martins, A.; Almeida, J.; Almeida, C.; Matias, B.; Kapusniak, S.; Silva, E. EVA a Hybrid ROV/AUV for Underwater Mining Operations Support. In Proceedings of the 2018 OCEANS—MTS/IEEE Kobe Techno-Oceans (OTO), Kobe, Japan, 28–31 May 2018.
- Araya, A.; Kanazawa, T.; Shinohara, M.; Yamada, T.; Fujimoto, H.; Iizasa, K.; Ishihara, T. Gravity gradiometer implemented in AUV for detection of seafloor massive sulfides. In Proceedings of the 2012 Oceans, Hampton Roads, VA, USA, 14–19 October 2012.
- Dunbabin, M.; Roberts, J.; Usher, K.; Winstanley, G.; Corke, P. A Hybrid AUV Design for Shallow Water Reef Navigation. In Proceedings of the 2005 IEEE International Conference on Robotics and Automation, Barcelona, Spain, 18–22 April 2005; pp. 2105–2110, ISBN 0-7803-8914-X.

10. Eichhorn, M.; Ament, C.; Jacobi, M.; Pfuetzenreuter, T.; Karimanzira, D.; Bley, K.; Boer, M.; Wehde, H. Modular AUV System with Integrated Real-Time Water Quality Analysis. *Sensors* **2018**, *18*, 1837. [[CrossRef](#)]
11. Sato, Y.; Maki, T.; Kume, A.; Matsuda, T.; Sakamaki, T.; Ura, T. Path replanning method for an AUV in natural hydrothermal vent fields: Toward 3D imaging of a hydrothermal chimney. *Mar. Technol. Soc. J.* **2014**, *48*, 104–114. [[CrossRef](#)]
12. Jaulin, L. A nonlinear set membership approach for the localization and map building of underwater robots. *IEEE Trans. Robot.* **2009**, *25*, 88–98. [[CrossRef](#)]
13. Maki, T.; Sato, Y.; Matsuda, T.; Shiroku, R.-T.; Sakamaki, T. AUV Tri-TON 2: An intelligent platform for detailed survey of hydrothermal vent fields. In Proceedings of the 2014 IEEE/OES Autonomous Underwater Vehicles (AUV), Oxford, MS, USA, 6–9 October 2014; pp. 1–5, ISBN 978-1-4799-4344-9.
14. Pyo, J.; Cho, H.; Joe, H.; Ura, T.; Yu, S.C. Development of hovering type AUV “Cyclops” and its performance evaluation using image mosaicing. *Ocean Eng.* **2015**, *109*, 517–530. [[CrossRef](#)]
15. Carreras, M.; Hernández, J.D.; Vidal, E.; Palomeras, N.; Ribas, D.; Ridao, P. Sparus II AUV—A Hovering Vehicle for Seabed Inspection. *IEEE J. Ocean. Eng.* **2018**, *43*, 344–355. [[CrossRef](#)]
16. Farrell, J.A.; Pang, S.; Li, W.; Arrieta, R.M. Biologically inspired chemical plume tracing demonstrated on an autonomous underwater vehicle. In Proceedings of the 2004 IEEE International Conference on Systems, Man and Cybernetics, Hague, The Netherlands, 10–13 October 2004.
17. Yildiz, Ö.; Gökalp, R.B.; Yilmaz, A.E. A review on motion control of the underwater vehicles. In Proceedings of the 2009 International Conference on Electrical and Electronics Engineering-ELECO 2009, Bursa, Turkey, 5–8 November 2009.
18. Jun, S.W.; Lee, H.J. Design of TS fuzzy-model-based controller for depth control of autonomous underwater vehicles with parametric uncertainties. In Proceedings of the 2011 11th International Conference on Control, Automation and Systems, Gyeonggi-do, Korea, 26–29 October 2011.
19. Dahmani, H.; Chadli, M.; Rabhi, A.; El Hajjaji, A. Road curvature estimation for vehicle lane departure detection using a robust Takagi–Sugeno fuzzy observer. *Veh. Syst. Dyn.* **2013**, *51*, 581–599. [[CrossRef](#)]
20. Medagoda, L.; Williams, S.B. Model predictive control of an autonomous underwater vehicle in an in situ estimated water current profile. In Proceedings of the 2012 Oceans-Yeosu, Yeosu, Korea, 21–24 May 2012.
21. Steenson, L.V. Experimentally Verified Model Predictive Control of a Hover-Capable AUV. Ph.D. Thesis, University of Southampton, Southampton, UK, 2013.
22. Zeinali, M.; Notash, L. Adaptive sliding mode control with uncertainty estimator for robot manipulators. *Mech. Mach. Theory* **2010**, *45*, 80–90. [[CrossRef](#)]
23. Kumar, N.; Panwar, V.; Sukavanam, N.; Sharma, S.P.; Borm, J.-H. Neural network-based nonlinear tracking control of kinematically redundant robot manipulators. *Math. Comput. Model.* **2011**, *53*, 1889–1901. [[CrossRef](#)]
24. Fallaha, C.J.; Saad, M.; Kanaan, H.Y.; Al-Haddad, K. Sliding-Mode Robot Control with Exponential Reaching Law. *IEEE Trans. Ind. Electron.* **2011**, *58*, 600–610. [[CrossRef](#)]
25. Feng, Y.; Zhou, M.; Han, F.; Yu, X. Speed Control of Induction Motor Servo Drives Using Terminal Sliding-Mode Controller. In *Advances in Variable Structure Systems and Sliding Mode Control—Theory and Applications*; Springer: Berlin/Heidelberg, Germany, 2018; pp. 341–356.
26. Yang, L.; Yang, J. Nonsingular fast terminal sliding-mode control for nonlinear dynamical systems. *Int. J. Robust Nonlinear Control* **2011**, *21*, 1865–1879. [[CrossRef](#)]
27. Brahmi, B.; Laraki, M.H.; Brahmi, A.; Saad, M.; Rahman, M.H. Improvement of sliding mode controller by using a new adaptive reaching law: Theory and experiment. *ISA Trans.* **2019**. [[CrossRef](#)]
28. Liu, J.; Yu, H.; Xu, Y. Improved S Plane Control Algorithm for Underwater Vehicles. *J. Harbin Eng. Univ.* **2002**, *23*, 33–36.
29. Fossen, T.I. *Handbook of Marine Craft Hydrodynamics and Motion Control*; John Wiley & Sons: Hoboken, NJ, USA, 2011; ISBN 1119991498.
30. Paull, L.; Saeedi, S.; Seto, M.; Li, H. AUV Navigation and Localization: A Review. *IEEE J. Ocean. Eng.* **2014**, *39*, 131–149. [[CrossRef](#)]
31. Zhang, G.-C.; Huang, H.; Qin, H.-D.; Wan, L.; Li, Y.-M.; Cao, J.; Su, Y.-M. A novel adaptive second order sliding mode path following control for a portable AUV. *Ocean Eng.* **2018**, *151*, 82–92. [[CrossRef](#)]

32. Liang, X.; Wan, L.; Blake, J.I.; Shenoi, R.A.; Townsend, N. Path following of an Underactuated AUV Based on Fuzzy Backstepping Sliding Mode Control. *Int. J. Adv. Robot. Syst.* **2016**, *13*, 122. [[CrossRef](#)]
33. Wang, N.; Sun, Z.; Zheng, Z.; Zhao, H. Finite-Time Sideslip Observer-Based Adaptive Fuzzy Path-Following Control of Underactuated Marine Vehicles with Time-Varying Large Sideslip. *Int. J. Fuzzy Syst.* **2018**, *20*, 1767–1778. [[CrossRef](#)]



© 2019 by the authors. Licensee MDPI, Basel, Switzerland. This article is an open access article distributed under the terms and conditions of the Creative Commons Attribution (CC BY) license (<http://creativecommons.org/licenses/by/4.0/>).